*Proc. Roy. Soc. Lond.* A. **313**, 453–475 (1969)
*Printed in Great Britain*

# Electrically driven jets

By Sir Geoffrey Taylor, F.R.S.

With an appendix by
M. D. Van Dyke

(*Received* 26 *March* 1969)

[Plates 3 to 8]

Fine jets of slightly conducting viscous fluids and thicker jets or drops of less viscous ones can be drawn from conducting tubes by electric forces. As the potential of the tube relative to a neighbouring plate rises, viscous fluids become nearly conical and fine jets come from the vertices. The potentials at which these jets or drops first appear was measured and compared with calculations.

The stability of viscous jets depends on the geometry of the electrodes. Jets as small as 20 $\mu$m in diameter and 5 cm long were produced which were quite steady up to a millimetre from their ends. Attempts to describe them mathematically failed. Their stability seems to be due to mechanical rather than electrical causes, like that of a stretched string, which is straight when pulled but bent when pushed.

Experiments on the stability of water jets in a parallel electric field reveal two critical fields, one at which jets that are breaking into drops become steady and another at which these steady jets become unsteady again, without breaking into drops.

Experiments are described in which a cylindrical soap film becomes unstable under a radial electric field. The results are compared with calculations by A. B. Basset and after a mistake in his analysis is corrected, agreement is found over the range where experiments are possible. Basset's calculations for axisymmetrical disturbances are extended to those in which the jet moves laterally. Though this is the form in which the instability appears, calculations about uniform jets do not seem to be relevant.

In an appendix M. D. Van Dyke calculates the attraction between a long cylinder and a perpendicular plate at a different potential.

It was pointed out 369 years ago by William Gilbert (1600) that a spherical drop of water on a dry surface is drawn up into a cone when a piece of rubbed amber is held at a suitable distance above it. This phenomenon has recently (Taylor 1964) been subjected to theoretical treatment and it was shown that a conducting fluid can exist in equilibrium in the form of a cone under the action of an electric field but only when the semivertical angle is 49.3°. Apparatus was constructed in which the necessary field could be set up and very nearly conical fluid surfaces or interfaces between two fluids were formed for which the semivertical angle was close to 49.3°.

An uncharged drop in a uniform electric field is pulled out into a nearly spheroidal form which becomes unstable when the field reaches a maximum value $1.62\,(T/r_0)^{\frac{1}{2}}$ (Taylor 1964) and the drop has become 1.85 times as long as its equatorial diameter. Here the field was expressed in e.s. units and $T$ the surface tension and $r_0$, the initial radius, are expressed in c.g.s. units. The same analysis predicts possible equilibrium shapes which are longer than 1.85 times the diameter though the corresponding

value of the field is less than 1.62 $(T/r_0)^{\frac{1}{2}}$. At higher fields the drop does not in fact pass through approximately spheroidal shapes, but develops pointed ends at which narrow jets appear or small drops are torn off. Several authors (Zeleny 1917; Magarvey & Outhouse 1962; Vonnegut & Neubauer 1952) have described experiments with such jets, but have not given theoretical discussions of their mechanics, perhaps because they could not relate the electric field to the geometry of their apparatus, even before the jet appeared. The experiments to be described were undertaken in the hope of being able to supply a rational description of the mechanics of these jets but complete success in that direction has not been attained. Nevertheless, some points of interest have appeared.

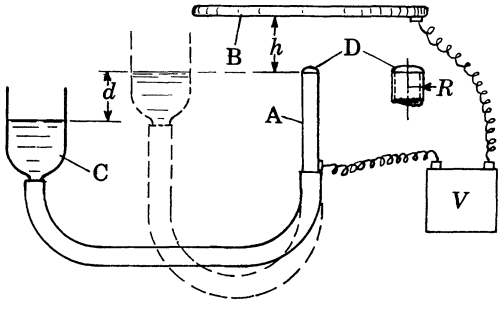


FIGURE 1. Sketch showing the geometry of the single plate apparatus used by Zeleny.

Most of the experiments so far recorded have been performed with apparatus sketched in figure 1 (Zeleny 1914; Magarvey & Outhouse 1962; Vonnegut & Neubauer 1952). Here A is an open-ended capillary tube of metal or glass containing a conducting fluid. Opposite it at a distance $h$ is a metal plate B. A and B are maintained at potential difference $V$ and the effects on the fluid surface at the open end of A observed as $V$ increases. Under these circumstances no theoretical calculation of the force which the electric field exerts on the fluids at the end of tube A had been made. Zeleny (1914), however, made measurements of the change in pressure which would keep the meniscus D (figure 1) in approximately a constant shape as $V$ changed. He measured the depth $d$ through which a reservoir C connected with the fluid in A had to be moved downward in order to maintain the meniscus D at a constant height as $V$ increased. He defined a mean electric field $f$, over the area of the top of the tube as being given by

$$f^2/8\pi = \rho g d, \tag{1}$$

and he thus measured $f$ as a function of $V$, $h$ and $R$ the radius of the tube. This method depends on the assumption that the shape of the meniscus remains spherical and though the assumption could only be true if the normal electric stress over the whole meniscus were uniform, it seems to be a good approximation because, as will be seen later, the observed connexion between $f$ and $V$ is very close to that calculated by Van Dyke, whose analysis is given in the appendix.

### Van Dyke's calculation

Van Dyke has calculated the attractive force $P$ between a long cylinder of length $L$ and radius $R$ and a perpendicular plane at distance $h$ when a potential $V$ is established between them. His calculations are given in the appendix and his results are displayed in figure 2 where $P/V^2$ is shown as a function of $h/R$ for constant values of $L/R$. It will be noticed in figure 2 that for a fixed value of $h/R$ the attractive force

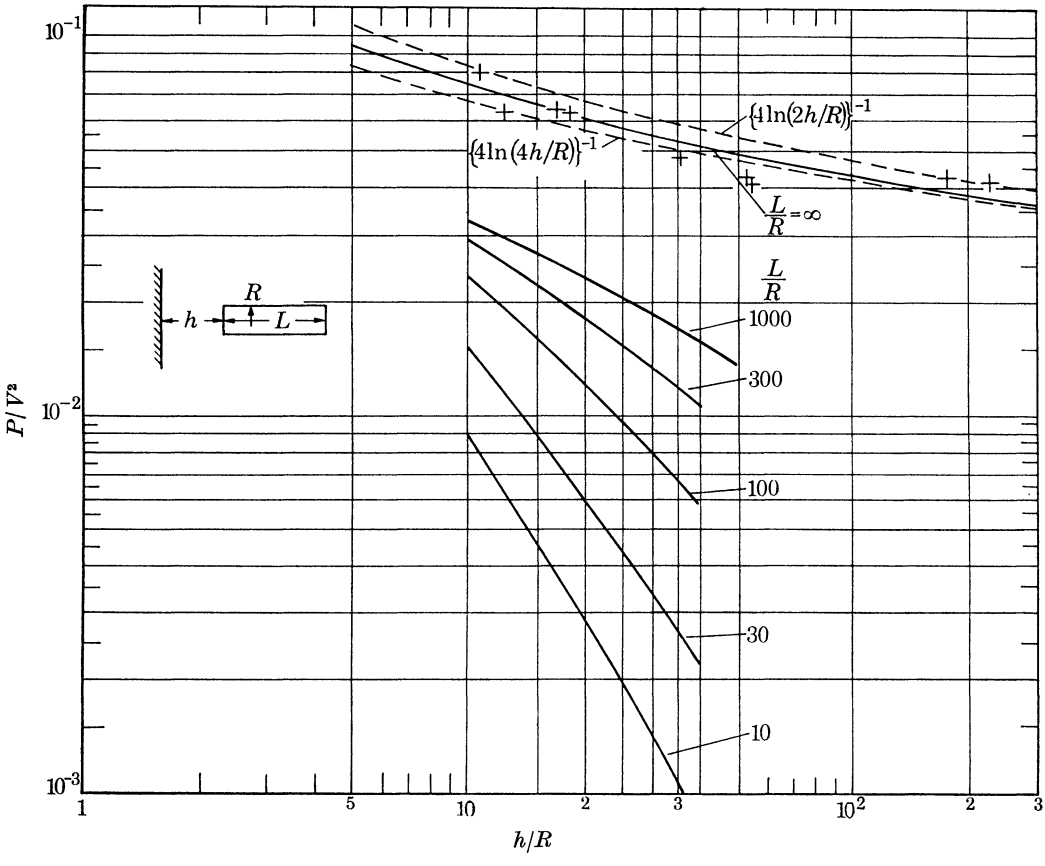


FIGURE 2. Van Dyke's calculation of the attraction between a plate and a cylinder of radius $R$ and length $L$ when separated by distance $h$. +, Experiments with single plate apparatus by Zeleny and by the present author. The upper broken line is $P/V^2 = \{4\ln(2h/R)\}^{-1}$ and the lower broken line $P/V^2 = \{4\ln(4h/R)\}^{-1}$.

increases as $L$ increases and that it is still increasing when $L/R$ is as great as 1000. When $L/R$ becomes infinite the analysis was difficult but it was carried out by computer for $h/R = 5$, 10, 33, 100, 1000. For all values of $h/R$ when $L/R$ is infinite, $P/V^2$ can be shown to lie between $1/\{4\ln(4h/R)\}$ and $1/\{4\ln(2h/R)\}$ which are fairly close limits when $h/R$ is large. The values computed by Van Dyke and these upper and lower bounds are given in table 1.

## Comparison of Van Dyke's calculation with Zeleny's measurements

Zeleny's measurements made with a tube a few centimetres long and radius 0.028 cm at $h = 0.5$, 1.0 and 1.5 cm were taken from figure 4 of his paper (Zeleny 1914) and are given in columns 2 and 3 of table 2. Here $V_k$ was expressed in kilovolts.

Table 1. Computed values of $P/V^2$ (column 2) for $L/R$ infinite

| | | bounds | |
|---|---|---|---|
| $h/R$ | computer | upper | lower |
| 5 | 0.0938 | 0.1086 | 0.0834 |
| 10 | 0.0744 | 0.0834 | 0.0678 |
| 33.33 | 0.0543 | 0.0593 | 0.0511 |
| 100 | 0.0435 | 0.0472 | 0.0417 |
| 1000 | 0.0308 | 0.0329 | 0.0301 |

$P$ was taken as $\pi R^2 g\rho d$ and given in column 4 of table 2. Column 5 gives $P/V^2 = P/(0.3\,V_k)^2$. The experimental points corresponding to column 5 of table 2 are marked in figure 2. It was be seen that they are in fairly good agreement with Van Dyke's calculation, a fact which may be taken as evidence that Zeleny's implied assumption that changes in the shape of the meniscus as $V$ increases do not appreciably effect his results provided the height above the top of the tube is kept constant.

Table 2. Zeleny's measurements of $V_k$ kilovolts and $d$ for tube $R = 0.028$ cm

| 1 | 2 | 3 | 4 | 5 | 6 |
|---|---|---|---|---|---|
| $h$ / cm | $V_k$ / kV | $d$ / cm | $P$ / dyn | $P/V^2$ | $h/R$ |
| 0.5 | 4.24 | 5.29 | 12.75 | 0.064 | 17.8 |
| 1.0 | 4.88 | 5.17 | 12.48 | 0.047 | 35.7 |
| 1.5 | 5.15 | 5.17 | 12.48 | 0.042 | 53.5 |

The agreement also confirms the implicit assumption that the attraction between fluid and plate does not depend on the field far from the end of the cylinder. The fact that Van Dyke's calculation for a cylinder 1000 times as long as its radius differs very appreciably from that of a cylinder for which $L/R$ is infinite is not surprising because Van Dyke's calculation was for the total force, that is the difference between the forces acting at the two ends. The force acting at the far end is still appreciable even when $L/R = 1000$. The force on the fluid is that which acts at the near end only and the implicit assumption that this depends only on the configuration in that neighbourhood can only be satisfied if the force is that on an infinite cylinder for the same value of $h/R$.

### Zeleny's measurements of the potential necessary for instability

In these experiments a pressure was applied to fluid in the tube A (figure 1) till the meniscus rose to a definite height above the end of the tube and this height was maintained by reducing the pressure, $p$, as the potential of A was increased till breakdown occurred and it was no longer possible to maintain the meniscus steady. Assuming that the fluid is a conductor and wets the top of the tube, the equation for the equilibrium of the part of the drop above the top is

$$2\pi RT\cos\phi + W = P + \pi R^2 p, \tag{2}$$

where $\phi$ is the angle which the fluid surface makes with the tube axis at the point

Table 3. Zeleny's measurements for critical voltage for instability when the meniscus was maintained at height $R$ above top of tube

| 1 | 2 | 3 | 4 | 5 | 6 |
|---|---|---|---|---|---|
| $\frac{R}{\text{cm}}$ | $\frac{h}{R}$ | $\frac{V_k}{\text{kV}}$ | $\frac{P\,(\text{van Dyke})}{\text{dyn}}$ | $\frac{\pi R^2 p}{\text{dyn}}$ | $\frac{P+\pi R^2 p}{2\pi RT}$ |
| 0.0543 | 27.6 | 5.9 | 21.3 | 3.3 | $\frac{24.6}{25} = 0.99$ |
| 0.0420 | 35.6 | 5.45 | 17.4 | 2.8 | $\frac{20.3}{19.5} = 1.04$ |
| 0.0340 | 44.1 | 4.0 | 13.9 | 1.9 | $\frac{15.8}{15.7} = 1.00$ |
| 0.0281 | 53.4 | 4.7 | 11.8 | 0.6 | $\frac{12.4}{13.0} = 0.95$ |
| 0.0231 | 64.8 | 4.50 | 10.3 | 0.6 | $\frac{10.9}{10.7} = 1.02$ |
| 0.0200 | 75 | 4.05 | 8.2 | 0.8 | $\frac{9.0}{9.3} = 0.97$ |
| 0.0166 | 90 | 4.05 | 8.0 | 0.7 | $\frac{8.7}{7.1} = 1.23$ |
| 0.0146 | 103 | 3.55 | 5.9 | 0.6 | $\frac{6.5}{6.7} = 0.97$ |

on the rim of the top where it leaves the tube and $W$ is the weight of the fluid above the top. In Zeleny's experiments $R$ was small enough to justify neglect of $W$. The results of experiments in which the height of the meniscus was equal to the radius, so that it was initially hemispherical, are given in table 3 which is taken from measurements displayed on p. 85 of Zeleny's paper (1914) in his figure 6. The values of the potential $V_k$ at which breakdown occurs is given in column 3 of table 3 and the calculated value of $P$, taken from figure 2, in column 4. To find $p$ it is necessary to take the values given in Zeleny's curves from the initial value

which, when the meniscus was initially hemispherical, was $2T/R$. Values of $\pi R^2 p$ found in this way are given in column 5. They were positive in all cases. According to (2) $\cos\phi = (P+\pi R^2 p)/2\pi RT$ and the values of this at breakdown are given in column 6. Except in one case they are very close to 1.0 so that when the experiment was carried out in Zeleny's way with a positive pressure behind the meniscus, breakdowns occur when $\phi$ is close to 90° and in all cases where the meniscus was initially hemispherical the value of $p$ at breakdown is small compared with its initial value.

*Two-plate apparatus*

Before Van Dyke's calculations had been made it was realized that a finite cylinder would have to be very long indeed before the total force on it was nearly the same as that on a semi-infinite cylinder. For this reason apparatus was constructed in which the electric field far from the tube containing the fluid would be

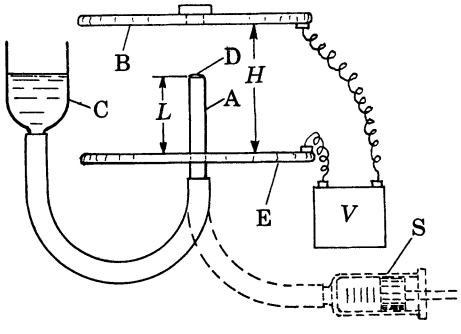


FIGURE 3. Geometry of the two-plate apparatus.

known so that it would not be necessary to assume that the distant field does not affect appreciably the force on the fluid emerging from its end. This apparatus shown in figure 3, consists of two parallel plates B and E separated by distance $H$ and maintained at potential difference $V_k$ kilovolts. Through the middle of the lower plate E passes the metal (hypodermic) tube A to a height $L$ and the fluid was supplied either from a reservoir C through a flexible tube or, if it was necessary to measure the rate of delivery, from a graduated syringe S connected through a metal pipe with A.

In the two-plate apparatus the value of the force $P$ exerted on a cylinder of length $L$ is (Taylor 1966)

$$P = \frac{V^2 L^2}{4H^2} \frac{1}{\ln(2L/R) - \frac{3}{2}}, \tag{3}$$

and (3) can be used in comparing experiments with theory.

### Experiments to determine the lowest value of $V$ at which fluid is drawn from the tube

In these experiments the reservoir C (figures 1 or 3) was first adjusted till the top of the fluid (D, figure 3) could be seen to reflect as a plane mirror so that $p = 0$. No further changes in pressure were made. The voltage was gradually increased and the surface of the meniscus became convex till at a certain voltage, $V_k$ kilovolts, static equilibrium could no longer be maintained. When water was used the breakdown of equilibrium developed into violent oscillations just as it does when a soap bubble is subjected to an electric field (Wilson & Taylor 1926). When very bad conductors such as transformer oil or silicone fluids were used drops came from the tube at infrequent intervals, detached themselves and rose. Figure 4, plate 3, shows the outline of a water drop in the single plate apparatus when $R = 0.163$ cm, $h = 1.58$ cm just before it became unstable at $V_k = 9.8$ kV. Using the curve of figure 2 the calculated value of $P$ was 85 dyn, and since $p = 0$ the equilibrium equation (2) is $P + W = 2\pi T \cos\phi$. The measured value of $\phi$ in figure 5 is 29.5° so that taking $T = 74\,\text{dyn cm}^{-1}$, $2\pi T \cos\phi = 66.4$ dyn. This is smaller than the calculated value of $P$, but part of the difference is due to the fact that $W$ is not negligible when $R$ is as large as 0.163 cm; in fact an estimate of $W$ is 8 dyn so that the calculated value of $P$, namely 85 dyn must be compared with $66.4 + 8 = 74.4$ dyn. It was thought that some of this discrepancy might be due to the fact that the plate used in the apparatus of figure 1 was not large enough to justify the use of a theory envisaging an infinite plate but enlargement of the plate did not affect the result appreciably. The agreement with theory was better when the two-plate apparatus was used. Measurements were made with the two-plate apparatus (figure 3) on a number of fluids and in each case the voltage at which drops first began to leave the top of the tube A when $p = 0$ was measured. It was found that when the fluid is conducting and sufficiently viscous the fluid does not vibrate but rises to a point. Figures 5 and 6, plate 3, show the appearance of the meniscus formed when a mixture of 95% glycerin mixed with 5% of a 10% sodium chloride solution was used. In figure 5 care was taken to ensure that $p = 0$ at the moment when the jet appeared at the top, but in figure 6 $p$ was a little higher. It will be seen that when $p = 0$ the meniscus is nearly conical with a semivertical angle close to the only possible equilibrium value 49.3° (Taylor 1964) and it will also be noticed that the surface remains nearly conical at the outer edge of the top of the tube, though this cannot be an accurate result derivable from theory. This observation however suggests that an approximate expression for predicting the critical potential at which jets or drops can appear when $p = 0$ can be put forward by setting $\phi = 49.3°$ in (2) and substituting for $P$ from (3). Since $2\cos 49.3° = 1.30$ this gives

$$V_k^2 = \frac{4H^2}{L^2}\left(\ln\frac{2L}{R} - \frac{3}{2}\right)(1.30\pi RT)\ (0.09). \tag{4}$$

The factor 0.09 is inserted to give the prediction in kilovolts. In table 4 details of a number of experiments conducted with $H = 7.66$ cm are recorded. The fluid as

well as $R$ and $L$ was varied but care was taken to ensure that $p = 0$. The results of the observed and computed values of $V_k$ using (4) are given in the last two columns of the table. The agreement is good in cases where the conical form appears before the jet forms, but it is also good in cases like that of figure 4 where the conical shape is not attained as a steady state.

TABLE 4. UPPER LIMIT OF STATICALLY STABLE MENISCUS IN TWO-PLATE APPARATUS WITH $H = 7.66$ cm AND $p = 0$.

| fluid | $R$/cm | $L$/cm | $V_k$/kV observed | $V_k$/kV calculated (eqn. (4)) |
|---|---|---|---|---|
| 1 | 0.05 | 2.1 | 13.0 | 13.4 |
| 1 | 0.05 | 3.0 | 9.5 | 10.0 |
| 2 | 0.05 | 1.5 | 17.5 | 17.6 |
| 2 | 0.05 | 2.5 | 11.5 | 11.6 |
| 2 | 0.162 | 3.0 | 13.0 | 14.2 |
| 3 | 0.12 | 21.0 | 17.5 | 17.8 |
| 3 | 0.12 | 3.0 | 14 | 13.2 |
| 4† | 0.05 | 3.0 | 14 | 14.2 |
| 4 | 0.05 | 2.2 | 14 | 13.9 |
| 4 | 0.05 | 3.55 | 9.5 | 9.4 |
| 4 | 0.12 | 3.0 | 14 | 14.2 |
| 4 | 0.12 | 2.0 | 17.5 | 17.8 |
| 4 | 0.12 | 3.0 | 14 | 14.2 |
| 5 | 0.163 | 3.0 | 11.4 | 11.0 |

† Oscillating jet shown in figure 7.

*Fluids*: 1. Glycerin, $T = 62.5$ dyn cm$^{-1}$.
2. 95 % glycerin, 5 % water, $T = 65$ dyn cm$^{-1}$.
3. 98 % glycerin, 2 % of 0.5 % NaCl solution.
4. Distilled water, $T = 73$ dyn cm$^{-1}$.
5. Transformer oil, $T = 37$ dyn cm$^{-1}$.

Figure 7, plate 3 for instance shows one of the cases listed in table 4. The oscillating drop is throwing off small drops. The agreement between the observed and calculated potentials is consistent with the experimental result (Taylor 1964) that there is little difference between the electric field which makes an isolated drop become unstable and the probably slightly lower field at which it can be pointed at the end.

## NON-CONDUCTING FLUIDS

When non-conducting fluids like transformer oil or silicones were used in either the single or double plate apparatus it was found that as the potential increased the meniscus was at first displaced in much the same way as for conducting fluids, but when the potential rose to the value at which a conducting fluid would become unstable and produce a fine jet, non-conducting fluids would throw off a drop and then after a considerable time another. Raising the potential above the critical

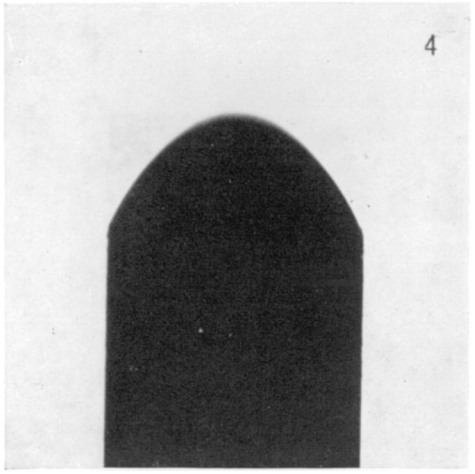


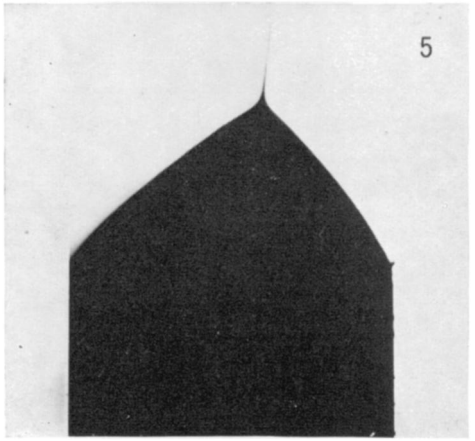


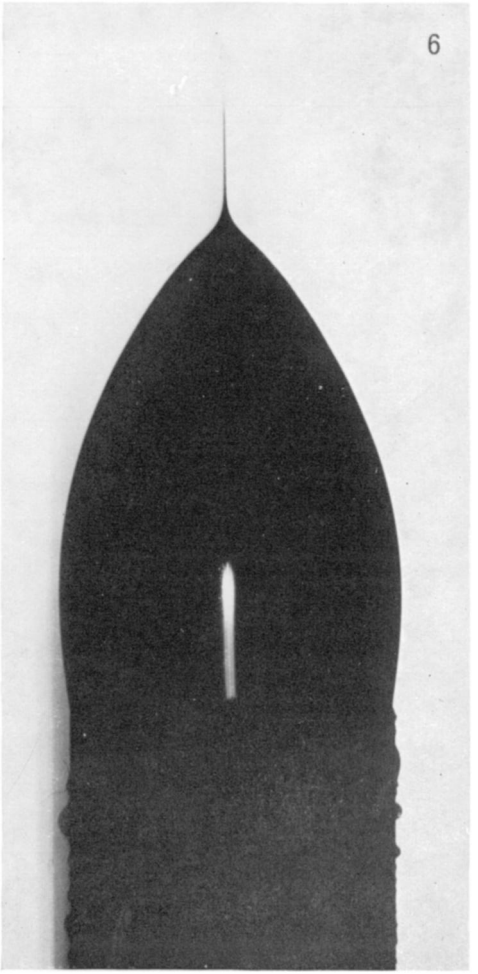


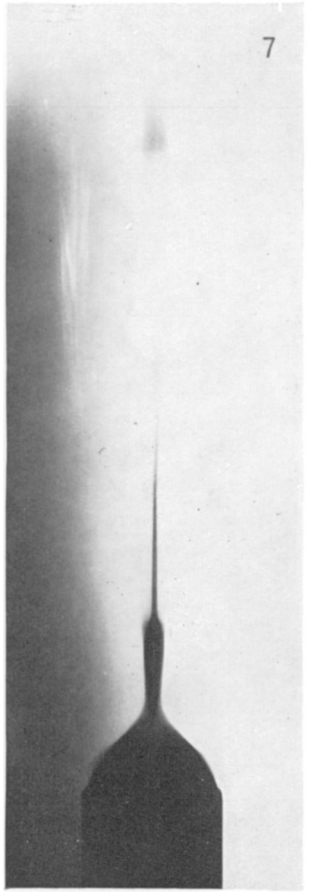


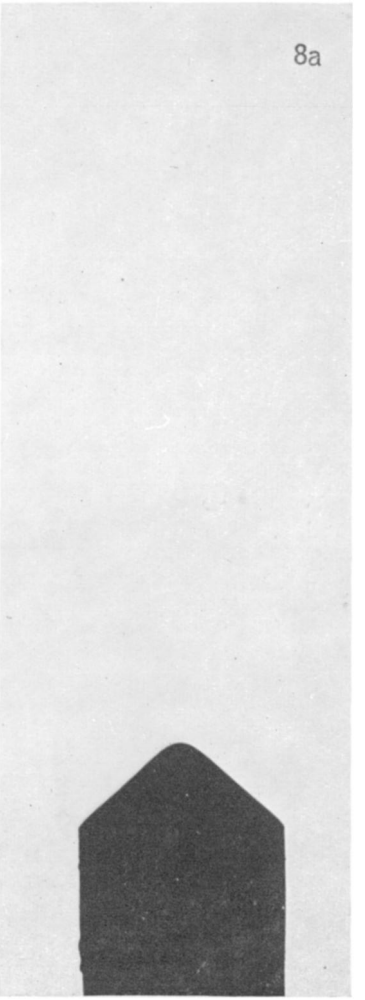


FIGURE 4. Water surface just before instability set in when $p = 0$.

FIGURE 5. Meniscus at the moment of jet formation. 95% glycerin, 5% dilute salt solution, $p = 0$.

FIGURE 6. Same conditions as figure 5 but $p$ positive.

FIGURE 7. Oscillating water jet in two-plate apparatus.

FIGURE 8($a$). Surface of Tellus oil ($\mu = 5$ P) at the top of metal tube ($R = 1.62$ mm, $L = 3.0$ cm, $H = 7.66$ cm) in two-plate apparatus just before instability set in.

(Facing p. 460)

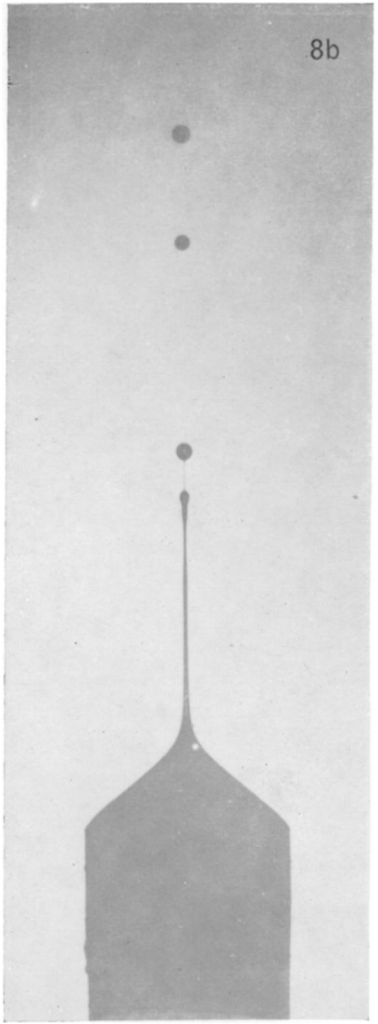


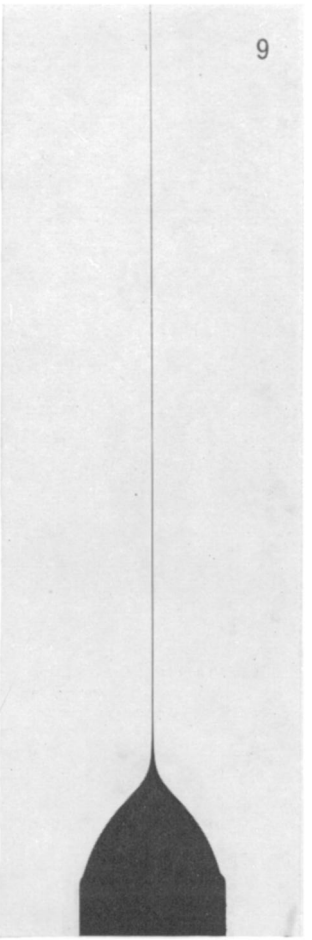


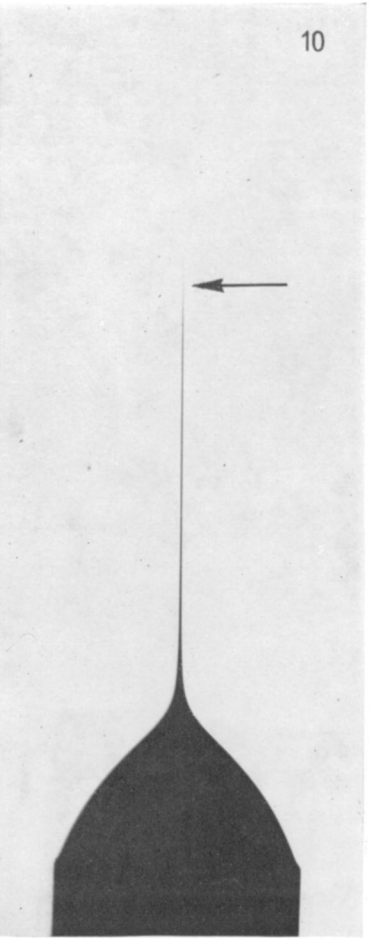


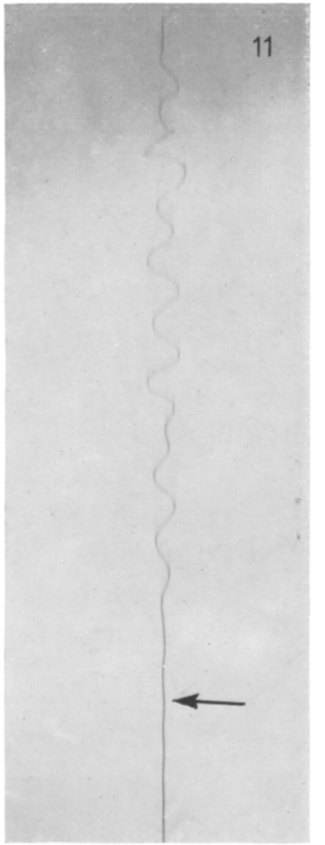


FIGURE 8 (*b*). Tellus oil, just after instability started.

FIGURE 9. First 1.4 cm of glycerin jet 4.66 cm long.

FIGURE 10. Jet 98 % glycerin, 2 % of 10 % NaCl solution, exposure time 1 ms.

FIGURE 11. Upper part of jet of figure 10, exposure time 2 $\mu$s.

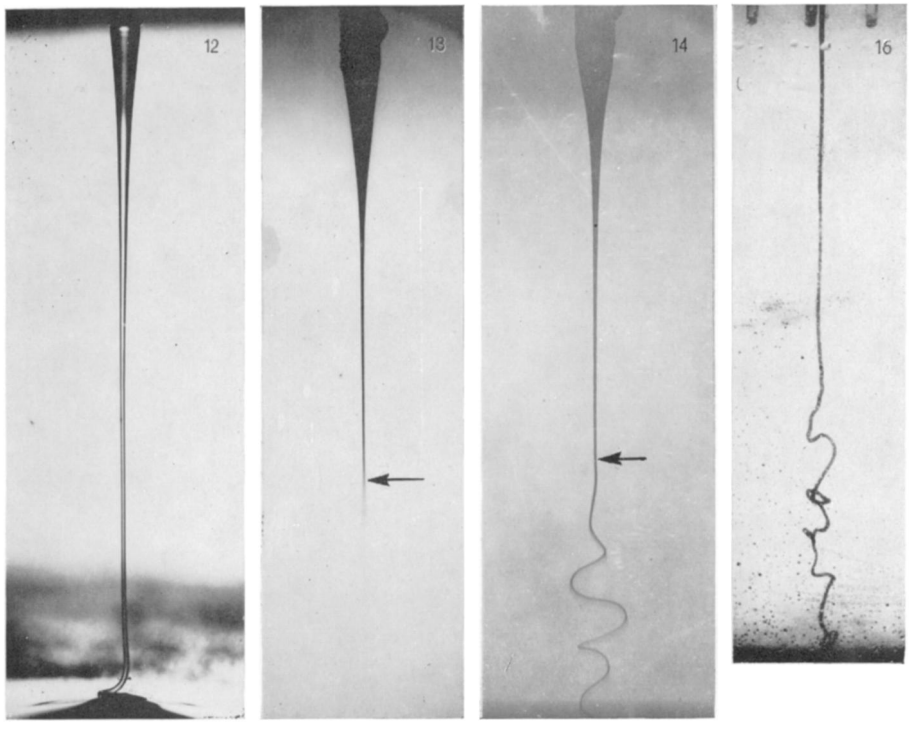


FIGURE 12. Jet of silicone (100 P) falling on a plate under gravity.

FIGURE 13. Downward jet of glycerin in a vertical field. Exposure 1 ms.

FIGURE 14. Same jet as in figure 13. Exposure 2 $\mu$s.

FIGURE 16. Glycerin jet made visible by indian ink falling in two layers of salt solution.

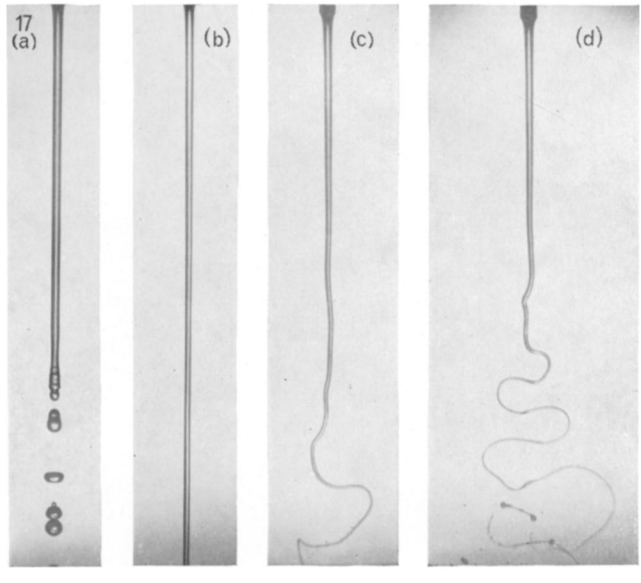


FIGURE 17. Water jet pointing down in two-plate apparatus. $Q = 0.28\,\mathrm{cm^3\,s^{-1}}$. $H = 5.5\,\mathrm{cm}$, $L = 1.7\,\mathrm{cm}$, $R = 0.053\,\mathrm{cm}$, $C = 0$, negative potential $V$ on lower plate, upper earthed. (*a*) $V = 0$, (*b*) $V = 10.7\,\mathrm{kV}$, (*c*) $V = 15\,\mathrm{kV}$, (*d*) $V = 17.5\,\mathrm{kV}$.

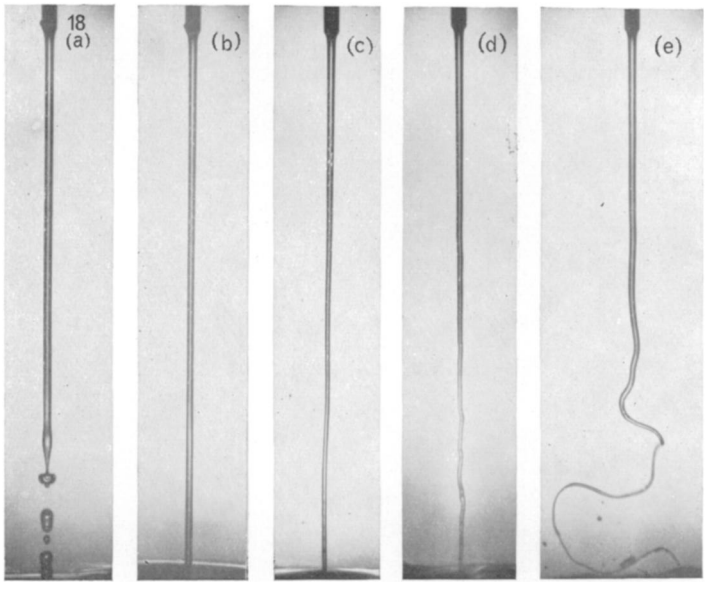


FIGURE 18. Dilute NaCl ($C = 2 \times 10^{-5}\,\mathrm{g\,cm^{-3}}$), $Q = 0.316\,\mathrm{cm^3\,s^{-1}}$, $H = 5.5$, $L = 1.7\,\mathrm{cm}$, $R = 0.053\,\mathrm{cm}$. (*a*) $V = 0$, (*b*) $V = 10$, (*c*) $V = 18$, (*d*) $V = 19\,\mathrm{kV}$, (*e*) $V = 20\,\mathrm{kV}$.

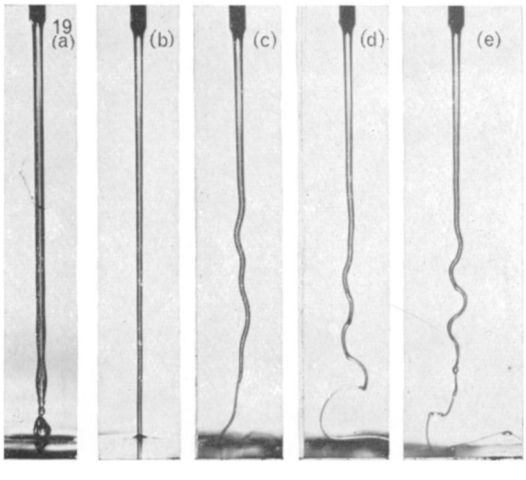


FIGURE 19. Water ($C = 0$). $Q = 0.255\,\mathrm{cm^3\,s^{-1}}$, $H = 5.5\,\mathrm{cm}$., $L = 2.8\,\mathrm{cm}$, $R = 0.053\,\mathrm{cm}$. (*a*) $V = 0$, (*b*) $V = 13\,\mathrm{kV}$, (*c*) $V = 14.5\,\mathrm{kV}$ (*d*) $V = 15.5\,\mathrm{kV}$. (*e*) $V = 19\,\mathrm{kV}$.

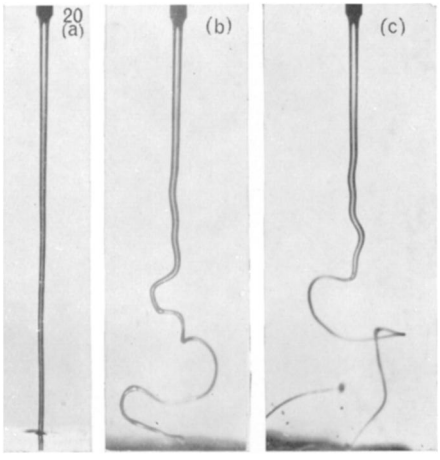


FIGURE 20. Dilute NaCl ($C = 10^{-5}\,\mathrm{g\,cm^{-3}}$). $Q = 0.255\,\mathrm{cm^3\,s^{-1}}$, $H = 5.5\,\mathrm{cm}$, $L = 2.28\,\mathrm{cm}$, $R = 0.053\,\mathrm{cm}$. (*a*) $V = 12\,\mathrm{kV}$, (*b*) $V = 13.5\,\mathrm{kV}$, (*c*) $V = 15\,\mathrm{kV}$.

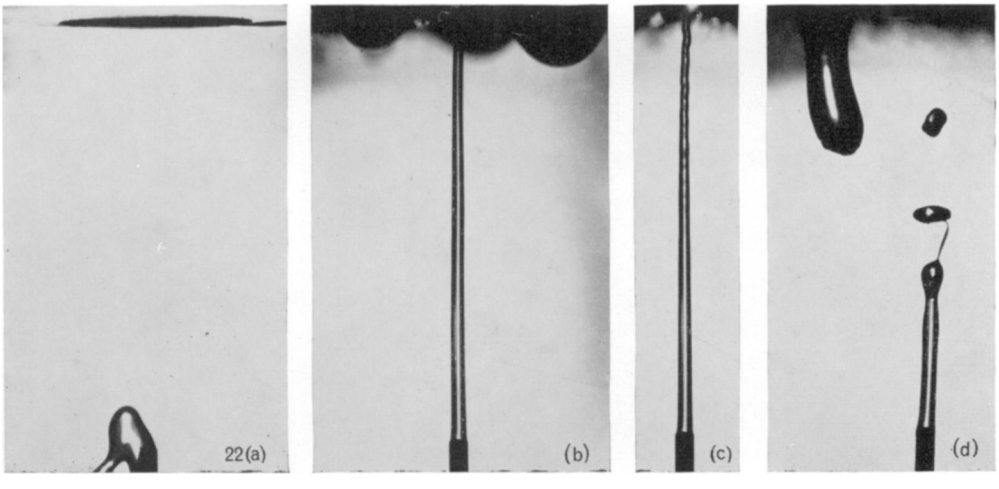


FIGURE 22. Water jet upwards. $Q = 0.466\,\mathrm{cm^3\,s^{-1}}$, $H = 5.5\,\mathrm{cm}$, $L = 2.7\,\mathrm{cm}$, $R = 0.067\,\mathrm{cm}$. (*a*) $V = 0$, (*b*) $V = 11\,\mathrm{kV}$. (*c*) $V = 12\,\mathrm{kV}$, (*d*) $V = 12\,\mathrm{kV}$.

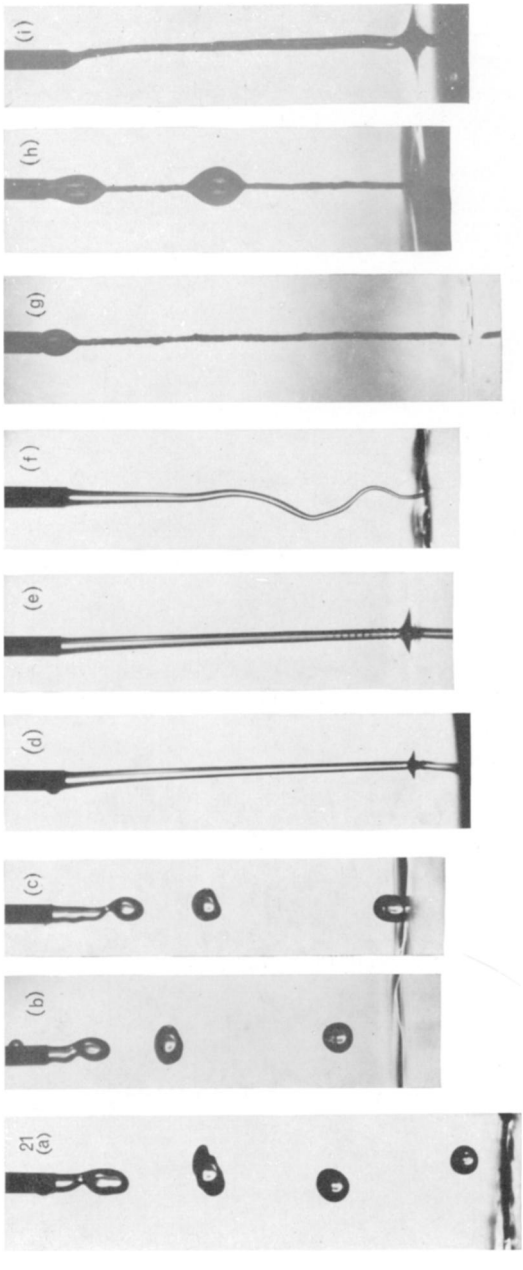


FIGURE 21. Water. $L = 2.75$ cm, $R = 0.067$ cm. (*a*) $H = 5.5$ cm, $Q = 0.37$ cm$^3$ s$^{-1}$, $V = 0$. (*b*) $H = 4.9$ cm, $Q = 0.37^3$ s$^{-1}$, $V = 3$ kV. (*c*) $H = 4.9$ cm, $Q = 0.37^3$ s$^{-1}$, $V = 6$ kV. (*d*) $H = 4.9$ cm, $Q = 0.37^3$ s$^{-1}$, $V = 7.8$ kV. (*e*) $H = 4.9$ cm, $Q = 0.37^3$ s$^{-1}$, $V = 4$ kV. (*f*) $H = 4.9$ cm, $Q = 0.37^3$ s$^{-1}$, $V = 17$ kV. (*g*) $H = 5.2$ cm, $Q = 0$, $V = 0$ silk thread. (*h*) $H = 4.9$ cm, $Q = 0.37$ cm$^3$ s$^{-1}$, $V = 0$ silk thread. (*i*) $H = 4.9$ cm, $Q = 0.37$ cm$^3$ s$^{-1}$, $V = 17$ kV silk thread.

value increased the rate at which drops were thrown off and sometimes when the potential rose very considerably perhaps to twice the critical value the drops might coalesce into a steady stream through this condition could only be attained by increasing the flow of liquid.

Figure 8 (*a*), plate 3, shows a meniscus of Tellus oil just before instability at the top of a steel tube 3.2 mm diameter. Figure 8 (*b*) shows the same jet when the voltage has been raised sufficiently to produce a stream of drops. When figure 8 (*a*) was taken the pressure at the level of the top of the jet was atmospheric ($p = 0$). For 8 (*b*), plate 4 no doubt the pressure was slightly less owing to the hydraulic resistance of the fluid flowing through the tube. Calculation, however, showed that this pressure drop would be small. The two photographs are interesting because they show that the nearly conical equilibrium form with semivertical angle 49.3° is set up in non-conductors (no doubt owing to a very small conductivity) as well as in conductors even though the electric field cannot be that which would be necessary for the establishment of a complete conical meniscus covering the whole of the cylindrical tube.

## Formation of steady streams

In the preceding pages the only force capable of moving the fluid which has been considered is the normal force which an electric field exerts on a conducting surface. A steady motion could not be produced in this way. In one of Zeleny's experiments (1917) performed with apparatus shown in figure 1, a jet of glycerine was produced which broke up into drops after traversing steadily a length of about 1.0 cm. It is possible, though perhaps unlikely, that such a jet might be drawn up by a normal force acting on the end of the continuous part of the fluid, but in experiments using glycerin in my two-plate apparatus (figure 3) jets were formed which extended in steady motion the full distance $H - L$ between the end of the tube A (figure 3) and the plate B, a distance up to 6 cm. These jets were so steady that an exposure of 1 s or more would reveal sharply a straight jet sometimes only 0.002 cm in diameter. Figure 9, plate 4, shows the first 1.4 cm of a jet of glycerin 4.66 cm long issuing from a tube projecting 3 cm into the space between two plates 7.66 cm apart. This jet was quite steady up to a point less than 0.1 cm from where it struck the upper plate. No doubt within a length comparable with its diameter it must have become unstable and piled up with an oscillating motion into a mound just as a thread of honey does when it falls on a plate, but this was too small to be visible.

### *Instability of viscous jets*

Under some circumstances a jet was observed which appeared to rise steadily for a short distance and then to disappear suddenly. Figure 10, plate 4, shows a case of this kind. Here an upward pointing jet of glycerin disappears at a height of 0.8 cm above the tube from which it originates. This disappearance can only be due to an instability setting in at about 0.8 cm at a frequency greater than the exposure time of 1 ms. Figure 11, plate 4, is a photograph of the same jet at the same

magnification but with an exposure time of about 2 $\mu$s. This photograph covers the blank space above the jet of figure 10 and an arrow is drawn in both figures 10 and 11 to mark the position 0.8 cm above the orifice where the instability seems to begin. This instability does not increase violently like that observed by Zeleny and others. It increases fairly rapidly at first and then stops increasing. No doubt the difference is due to the difference in the electric fields set up in the single and the two-plate apparatus. The explanation of this type of bending of the jet seems to be that owing to viscous stress it is straight like a stretched string while it is extending

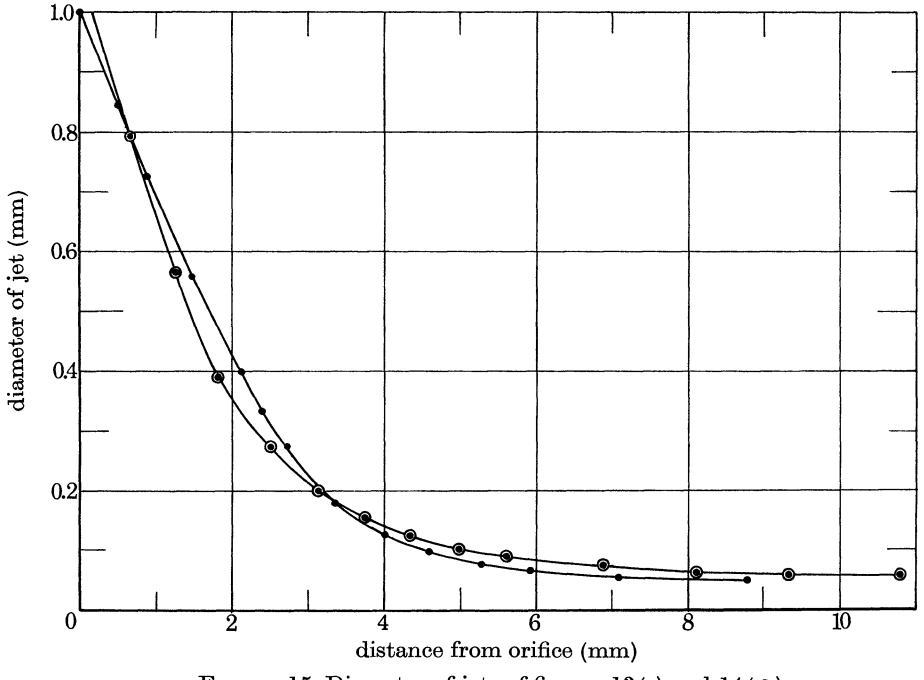


FIGURE 15. Diameter of jets of figures 13(•) and 14(⊙).

but that at a certain stage the electrostatic forces cease to be able to support it against gravity or tangential air friction so that it begins to slow down and therefore to contract longitudinally. The viscous stress therefore reverses. It then becomes unstable with an instability analogous to that of Euler when an elastic column is under end compression. A small amount of crumpling, however, relieves the compression so that it does not become violently unstable. The kind of instability just described is well known in the case of syrup falling on a plate but in that case the part of the falling jet which is under longitudinal compression is limited to a short distance from the point in which its velocity is reduced to zero. Figure 12, plate 5, for instance, shows a jet of a viscous fluid (a silicone) falling under gravity. The diameter of the jet decreases downwards till it reaches a short distance above the plate on which it spreads. It then thickens and begins to oscillate before it spreads out on the plate. When the jet is also pulled in the same direction as gravity

by electric forces it may acquire a speed greater than the limiting velocity at which tangential aerodynamic stress exactly balances gravity. Any decrease in electric stress will then give rise to a compressive longitudinal stress in the jet. Figure 13, plate 5, shows a downward jet of glycerine in a vertical field, photographed with exposure time 1 ms. Figure 14, plate 5, shows the same jet when the exposure is 2 $\mu$s. Measurements of the diameter of the steady part of the jets in these two photographs are shown in figure 15. It will be seen that though they are not quite identical the diameter stops decreasing just before the jet begins to oscillate at about 0.8 cm from the orifice. The fact that the diameter stops decreasing is evidence that the aerodynamic tangential drag has become equal to the sum of the forces due to electric attraction and gravity and one of the principal difficulties in attempting to give a quantitative theory of the electrically driven viscous jets is that of estimating the tangential aerodynamic drag even when the jet is quite steady as it is in figure 9.

*Experiment illustrating instability due to reversal of stress*

Figure 16, plate 5, shows a stream of glycerin of density 1.26, made visible by a mixture of indian ink, falling into a stratified salt solution whose density in the upper half is approximately 1.24 and 1.25 in the lower half. The driving force $1.26\,\mathrm{g} - 1.24\,\mathrm{g} = 0.02\,\mathrm{g}$ keeps the upper half in tension and therefore straight. In the lower half the driving force is $1.26\,\mathrm{g} - 1.25\,\mathrm{g} = 0.01\,\mathrm{g}$ and this is not sufficient to maintain the speed acquired in the upper half so the jet contracts longitudinally and becomes unstable owing to reversal of viscous stress. Figure 16 can be compared with figures 10 and 11. Figure 16 shows the tank with the 1 mm tube just projecting through the surface of the upper fluid. Above this is the top of the tank, held down by the screws into the Perspex sides which can be seen. The level of the interface between the two densities of salt solution shows faintly through dispersion of indian ink about half way down the jet.

*Stability of jets of water and dilute salt solution*

The effect of induced charges on water jets has often been studied. Plateau (1873) showed that in the absence of an electric field a uniform column of fluid is unstable under the influence of surface tension for all axisymmetric waves of length greater than the circumference of the cross section. Rayleigh (1879*a*) also discussed the axisymmetrical instability of flowing jets and showed experimentally that the columns broke into drops corresponding with the wavelength of maximum growth rate (1879*b*, 1891). He also commented (1879*b*) on the great effect which induced charges are observed to have in causing colliding drops to coalesce. Basset (1894) and Melcher (1963) extended calculations of the stability of axisymmetrical waves to conducting jets with known induced charge, and showed that the charge (under certain limiting conditions) has the effect of extending the range of stability to waves of length about 1.6 times the circumference. Basset confesses, however, that this result does not seem to explain what is observed. None of the workers in the subject has presented any satisfying explanation of why an induced charge

has a very powerful effect in preventing the break up of jets into drops under certain circumstances and an equally powerful effect in causing violent unsteady movements ultimately disintegrating the jet into drops in others (Zeleny 1917). I must confess that the experiments to be described fail also, but since they exhibit both these effects at different electric fields in the same apparatus it seems worth publishing photographs with the relevant data in the hope that someone may give a relevant analytical description of the stabilizing effect of induced charge on axisymmetric disturbances and the unstabilizing effect on disturbances which displace the jet laterally.

*Experiments with the two-plate apparatus*

In these experiments the plates were horizontal 30 cm diameter and 5.5 cm apart. Steel tubes of two sizes, 0.1 cm and 0.134 cm diameter, were used to supply the water and they projected to distances 1.7 and 2.7 cm from the plate sometimes pointing upwards and sometimes downwards. The measured quantities were $V$, the potential difference between the plates and $Q$ the volumetric rate of flow of the water. Most of the pictures were taken with single flashes of about 2 $\mu$s duration. In all cases when $Q$ was small enough the jets exhibited the Rayleigh–Plateau instability before the electric field was applied, and the jets broke into drops (figures 17*a*, 18*a*, 19*a*, 21*a*, plates 5, 6, 8). As $V$ or $Q$ increased or $R$ decreased the continuous part of the jet increased and at a certain potential a steady régime was established over the full length of the jet (figures 17*b*, 18*b*, 19*b*, 20*a*, 21*d*, plates 5 to 8). An increase in $V$ beyond a second critical value makes the jet become unsteady and whip about, particularly at its lower end (figures 17*c*, 17*d*, 18*d*, 18*e*, 19*c*, 19*d*, 19*e*, 20*b*, 20*c*, plates 5 to 7). This unsteadiness develops into very violent motion as $V$ increases. Such motions have often been reported (Magarvey & Outhouse 1962; Zeleny 1917), but in most cases the threads break into drops which repel one another. In the present experiments the threads of fluid remain continuous through the whole length from the tube to the opposite electrode. The fact that at a definite $V$ a steady stream becomes unsteady near its far end appears at first sight to be the same phenomenon as that observed with viscous conducting fluid, but in viscous jets the onset of instability seems to be associated with a reversal of the force over cross-sections near points where the sectional area is least. In the present experiments with water the effect of the field is to make the section decrease in area through the whole length of the jet and the onset of unsteady motion seems to be associated with a rapid decrease in jet diameter near the end where it strikes the electrode. To find whether the unsteadiness would occur if the cross section were prevented from decreasing at its lower end a fine silk thread (figure 21*g*, *h*, *i*, plate 8) was led through the tube in such a way that its lower end was just clear of the lower electrode but dipped into the water deposited on it by the jet. This device effectively prevented the fluid from accelerating and kept the diameter nearly constant without impeding possible lateral motion. When the water was turned on drops ran down the wet silk thread (figure 21*h*). An increase in potential of about the same magnitude as that which made the drops coalesce into a steady jet when there was no thread

had the same effect when the thread was present (figure 21*i*). Raising the potential up to and beyond the point where the free jet became violently unsteady had no effect on the threaded stream which remained steady till sparks jumped from the tube to the lower plate.

The effect of increasing $Q$ when there was no thread was to increase the potential necessary for unsteadiness to occur (compare figures 18*c* and 19*c*), but had little effect on the threaded jet (figure 20*i*). The water used had conductivity of order $10^{-8}\,\Omega^{-1}\,\mathrm{cm}^{-1}$ and it might be low enough to make the convected charge comparable with the conducted charge. Experiments were therefore made with dilute NaCl solution of concentrations $10^{-5}$ and $2\times10^{-5}\,\Omega^{-1}\,\mathrm{cm}^{-1}$. The currents increased very greatly but there was little change in the potential at which the jet began to be unsteady in the lower half of its path. Figures 19*b* and 19*c* show that unsteadiness with water began between 13 and 14.5 kV. Figure 20*b* shows that with the same value of $Q$ and the same geometry the jet is steady at 12 kV but unsteady at 13.5 kV when the salt concentration was $10^{-5}\,\mathrm{g\,cm}^{-3}$. It seems therefore that it would be justifiable to discuss these experiments assuming that the potential at any point in the jet depends only on the distribution of cross sections. For a given geometry and a given $Q$ the tangential stress on the jet depends only on the potential and the distribution of cross section along the jet so that the conductivity does not affect the stress which in turn determines the distribution of cross section along the jet.

After the stream had been made coherent and steady by raising the potential to a critical value it could remain steady when the potential was lowered. In figure 21*a*, *b*, *c* the potentials were 0, 3, 6 kV. At 7.8 kV the drops coalesced (figure 21*d*) and on lowering the potential to 4 kV (figure 21*e*) the stream remained steady and coherent though it became thicker at its lower end. When lowered to 3 kV it broke into drops and looked like figure 21*b*. At 17 kV (figure 21*f*) the jet had developed a considerable unsteadiness but remained coherent.

### *Upward jet*

When the jet was aimed upwards the water just rose a very short distance above the top of the tube from which it flowed and then fell down outside it (figure 22*a*). It was not possible to produce a steady stream with the flow rate $Q = 0.37\,\mathrm{cm}^3\,\mathrm{s}^{-1}$ used for figure 21 but at $Q = 0{\cdot}466\,\mathrm{cm}^3\,\mathrm{s}^{-1}$ and with the same geometry as for figure 21 a steady upward stream was produced at 11 kV (figure 22*b*). The experimental difficulty encountered with upward jets was that the water collected on the upper electrode formed hanging drops which fell and disturbed the electric field. This difficulty was overcome by cutting a hole 1.3 cm diameter in the upper plate on the axis of the jet (seen at the top of figure 22*a*). The jet disintegrated into drops immediately after passing the hole, and a shallow conical copper box was placed on the upper electrode to catch them. In spite of this precaution, however, some hanging drops were liable to occur. Some can be seen in figure 22*b*, but unless they coalesced and dropped off (figure 22*d*) they did not disturb the field enough to have a

visible effect on the jet when it became steady. It was noticeable that the potential required to make a steady upward jet was not very much larger than for a downward pointing jet, but the least possible value of $Q$ was greater.

## A POSSIBLE LINE OF THEORETICAL DISCUSSION

The instability of a charged liquid sphere, isolated in space, was shown to occur (Rayleigh 1879*b*) when the charge $C$ is greater than $(16\pi r^3 T)^{\frac{1}{2}}$. This has been verified experimentally (Doyle, Moffet & Vonnegut 1964). The instability for the least critical value of $C$ corresponds with a spheroidal form of the displaced surface. For the isolated sphere the critical charge coincided with the surface charge which was just sufficient to reduce the pressure inside the sphere to that of the surroundings. This result is not of more general application for it did not turn out to be true for the instability of an uncharged drop in a uniform field (Taylor 1964). Basset's calculation for the stability of a conducting cylinder of fluid of radius $a$ at rest assumes a varicose disturbance,

$$r = a + b\cos mx\, e^{\kappa t}. \tag{5}$$

Using a form of associated Bessel function $K_n(z)$ which differs from that used by Watson (1922) in the sign of $K_0(z)$, he finds the equation for $K$

$$\frac{\kappa^2 \rho a\, I_0(ma)}{maI_1(ma)} = -\frac{T}{a^2}(m^2a^2 - 1) - \frac{E^2}{4\pi a^2}\left(1 + \frac{maK_1(ma)}{K_0(ma)}\right), \tag{6}$$

where $I_0(z)$, $I_1(z)$, $K_0(z)$, $K_1(z)$ are associated Bessel functions. $E$ is the charge per unit length.

Using the same symbols defined as in Watson's treatise (1922) where these functions are all positive, I find

$$\frac{\kappa^2 \rho a I_0(ma)}{maI_1(ma)} = -\frac{T}{a^2}(m^2a^2 - 1) - \frac{E^2}{\pi a^3}\left(1 - \frac{maK_1(ma)}{K_0(ma)}\right). \tag{7}$$

This differs from (6) in the factor $E^2/4\pi a^2$ which in my calculations is $E^2/\pi a^3$. The difference may not be important in qualitative discussion, but is of importance when comparing calculation with experiments.

As Basset points out, large charges tend to produce instability ($\kappa^2$ positive) when $ma > 0.6$ and stability ($\kappa^2$ negative) when $ma < 0.6$. It is only when

$$0.6 < ma < 1.0$$

that no values of $E$ can stabilize the cylindrical fluid. Basset remarks that his result does not explain why it is that a very *slight* charge produces the stability described by Rayleigh. The experiment to which this remark refers was concerned with the large stabilizing effect of a small difference in *potential* between the jet and its distant surroundings. The induced charge was not measured.

EXPERIMENTS ON THE STABILITY OF A CYLINDRICAL FILM

In view of the difficulties Rayleigh and others have found in accounting for the stability characteristic of a cylindrical liquid conductor in a radial field it seemed worth while to construct apparatus for producing a cylindrical soap film. Such a film can be produced when the total length is less than its circumference, and its stability under a radial field can be examined because the wavelength of a varicose instability is simply the length between the fixed supports of the film. The difficulty

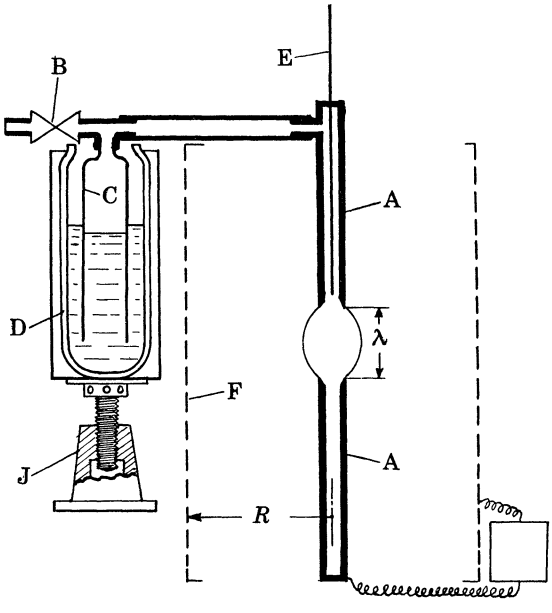


FIGURE 23. Apparatus for producing a cylindrical soap film and subjecting it to a radial field.

experienced in analysing the experiments with jets in the two-plate apparatus (that no method for calculating the charge induced on the jet has been found) can be overcome by surrounding the cylindrical film and the cylindrical conductors between which the film is held by a cylindrical conducting screen F, of radius $R$ which is many times the radius $a$ of the film. In this case the charge $E$ per unit length is connected with $V$ the potential difference between the cylinder and the screen by the equation

$$E = V/2\ln(R/a), \tag{8}$$

so that measurements of $R$ and $a$ determine $E$. The apparatus is shown in figure 23. Two copper tubes A, A, sharpened at the ends, are held coaxially in non-conducting supports so that the distance $\lambda$ between them can be controlled. The lower one is closed at its lower end. The upper one is connected by non-conducting tube to an open ended vessel, C which is inverted in a vacuum flask D containing water which can be raised or lowered by a jack J and it forms a simple means of controlling the

volume of air in the film which is produced in the space $\lambda$ (figure 23) between the tubes. Soap films were laid over the ends of the copper tubes and a bubble is blown through the stopcock B till it touches the film stretched over the lower tube. A rod E (figure 23) is then lowered to pierce the lower film. The stopcock is opened slightly and the bubble allowed to collapse till it is nearly cylindrical. The stopcock is closed and the fine adjustment provided by lowering the jack makes it possible to obtain a truly cylindrical film. The potential is then raised without further adjustment of the volume and was found that the film remains cylindrical till,

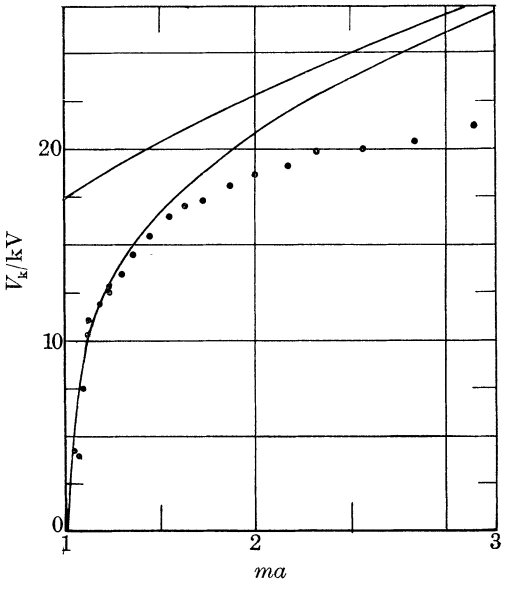


FIGURE 24. Potential necessary to produce instability on a cylindrical soap film 1.35 cm diameter inside a wide screen 13 cm diameter. Lower curve, axisymmetric disturbances. Upper curve, disturbances with lateral displacement. •, Experimental points.

at a certain potential which was measured, it bursts. Experiments were carried out in the range $1.0 < ma < 3.2$ and it was found that in the upper part of this range $ma > 1.5$ the film oscillated violently before bursting but the point at which the burst occurred could be measured within a small percentage.

The diameter of the copper tubes AA was 1.35 cm and that of the surrounding wire screen was 13 cm so that for the apparatus used

$$V = E(2 \ln 9.6) = 4.523E,$$

expressed in electrostatic units. The values of $V$ were measured in kilovolts, $V_k$, each of which is 1/0.3 electrostatic units so that

$$V_k = 1.357E.$$

Calculated value of $V_k$ for neutral stability is therefore

$$V_k = 1.357\,(\pi aT)^{\frac{1}{2}}\,(ma^2a^2 - 1)^{\frac{1}{2}} \left(\frac{maK_1(ma)}{K_0(ma)} - 1\right)^{-\frac{1}{2}} \tag{9}$$

The surface tension of the soap solution used was 27 dyn cm$^{-1}$ so that $T = 54$ and $(\pi aT)^{\frac{1}{2}} = 10.700$ so that

$$V_k = 14.50\,(m^2a^2-1)^{\frac{1}{2}}\left(\frac{maK_1(ma)}{K_0(ma)}-1\right)^{-\frac{1}{2}}. \tag{10}$$

The values calculated from (10) and the observed potentials at which the cylindrical soap film burst are shown in figure 24.

## Instability in mode which moves the whole jet laterally

Referring to figures 17 and 22 it seems that when the steady jet becomes unstable owing to large induced charge the displacement is one which moves the jet laterally rather than causing varicose swellings. Such a jet would be represented by

$$r = a + b\,e^{\kappa t}\cos mx\cos\theta, \tag{11}$$

where $r$, $x$, $\theta$ are cylindrical coordinates.

Applying the same methods that Basset used for discussing the varicose instability the equation for $\kappa^2$ analogous to (7) appears to be

$$\frac{\kappa^2 a\rho\, I_1 ma)}{maI_1'(ma)} = -m^2a^2\left(\frac{T}{a^2}\right)-\frac{E^2}{\pi a^3}\left(1+\frac{maK_1'(ma)}{K_1(ma)}\right). \tag{12}$$

Using Watson's (1922) definitions of $I_n(z)$, $K_n(z)$ and recurrence formulae

$$\left.\begin{aligned}\frac{maI_1'(ma)}{I_1(ma)} &= \frac{maI_0(ma)}{I_1(ma)}-1\\ \text{and}\qquad 1+\frac{maK_1'(ma)}{K_1(ma)} &= \frac{-maK_0(ma)}{K_1(ma)},\end{aligned}\right\} \tag{13}$$

we can write (13) in a form convenient for use with Watson's tables, namely

$$\kappa^2 a\rho\Big/\left(\frac{maI_0(ma)}{I_1(ma)}-1\right) = -m^2a^2\left(\frac{T}{a^2}\right)+\frac{E^2}{\pi a^3}\left(\frac{maK_0(ma)}{K_1(ma)}\right), \tag{14}$$

and the neutral stability condition

$$E^2 = \pi aT\left\{\frac{maK_1(ma)}{K_0(ma)}\right\}. \tag{15}$$

The interior is at atmospheric pressure when $E^2 = 2\pi aT$.

For small values of $ma$, the term $maI_0(ma)/I_1(ma)-1$ tends to the value 1.0, so that for long waves the left-hand side of (14) is $k^2a\rho$. When $E = 0$, $k = -m^2T/a\rho$ thus the configuration is stable and waves travel at velocity $ik/m = (T/a\rho)^{\frac{1}{2}}$.

Comparing this with the waves in stretched string whose velocity is (tensile force/mass per unit length)$^{\frac{1}{2}}$ the tensile force is $2\pi aT-\pi a^2$ (pressure) and the pressure is $T/a$ so that the tensile force over each section is $\pi aT$ and the mass per unit length is $\pi a^2\rho$ so that the velocity of waves is $(\pi aT/\pi a^2\rho)^{\frac{1}{2}} = (T/a\rho)^{\frac{1}{2}}$. Though this may serve as a confirmation of the correctness of the mathematics, it is of little practical value since the varicose instability relative to cylinders of fluid at rest

prevents such waves from being observed when the length unsupported is greater than $2\pi a$.

For the neutral stability of disturbances of a cylindrical soap film of diameter 13.5 cm in the mode represented by (11) the equations analogous to (10) is

$$V_k = 14.5\left\{\frac{maK_1(ma)}{K_0(ma)}\right\}^{\frac{1}{2}}. \tag{16}$$

The calulated values are also shown in figure 24. It will be seen that the potential necessary for instability in this mode is always higher than that required for instability in the varicose mode when $ma > 1.0$.

In the range $0 < ma < 0.6$ the electric field could theoretically stabilize the Rayleigh varicose instability. Thus for the soap film cylinders of diameter 1.35 cm the following potentials would be necessary to prevent the Rayleigh varicose instability from occurring.

| $ma$ | 0 | 0.1 | 0.2 | 0.3 | 0.5 |
|---|---|---|---|---|---|
| $V_k$ | 14.5 | 18.7 | 21.1 | 24.0 | 39 |

but this condition cannot be achieved physically with the apparatus shown in figure 23, because axisymmetric waves whose lengths are submultiples of the distance between the copper tubes and are in the range $ma > 1$, require less potential to make them unstable than is necessary to stabilize them against the Rayleigh varicose instability in the range $0 < ma < 0.6$.

My thanks are due to Professor van Dyke for writing the appendix and to Mr Tillet for verifying my statement that Basset calculation is erroneous.

## References

Basset, A. B. 1894 *Am. J. Math.* **16,** 93.
Doyle, A., Moffet, D. R. & Vonnegut, B. 1964 *J. Coll. Sci.* **19,** 136.
Gilbert, W. 1600 *de Magnete*, Book 2, chap. 2 (Trans. by P. F. Mottelay.)
Margavey, R. H. & Outhouse, L. E. 1962 *J. Fluid Mech.* **13,** 151–157.
Melcher, J. R. 1963 *Fluid coupled surface waves*, chap. 6. Cambridge, Mass.: Mass Inst. Tech. Press.
Plateau 1873 *Statique Experimentale et theoretique soumis aux seules forces moleculaire*, vol. II, p. 254.
Rayleigh 1879*a* *Proc. Lond. Math. Soc.* **10,** 473.
Rayleigh 1879*b* *Proc. Roy. Soc.* **28,** 406–409.
Rayleigh 1891 *Nature, Lond.* **44,** 249–254.
Taylor, G. I. 1964 *Proc. Roy. Soc. Lond.*, A **280,** 383–397.
Taylor, G. I. 1966 *Proc. Roy. Soc. Lond.*, A **291,** 145–158.
Vonnegut B. & Neubauer, R. L. 1952 *J. Coll. Sci.* **7,** 616.
Watson, G. N. 1922 *Bessel functions*. p. 79. Cambridge University Press.
Wilson, C. T. R. & Taylor, G. I. 1926 *Proc. Camb. Phil. Soc.* **22,** 728–730.
Zeleny J. 1914 *Phys. Rev.* **3,** 69–91.
Zeleny, J. 1917 *Phys. Rev.* **10,** 1–6.

# APPENDIX. THE ELECTROSTATICS OF A NEEDLE NORMAL TO A PLANE

By M. D. Van Dyke

We consider a charged needle normal to a nearby uncharged plane, using the notation shown in figure A 1. We admit the limiting cases of an isolated needle ($h \to \infty$) and a semi-infinite one ($L \to \infty$). Except near a very blunt end, the field can

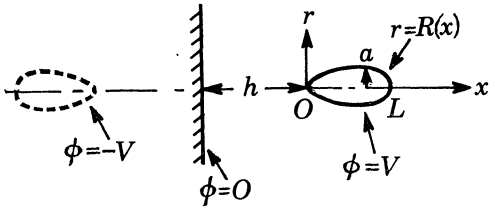


Figure A 1

be represented by a continuous distribution $\sigma(x)$ of charge along the axis of the needle. By the method of images this is seen to satisfy the integral equation

$$\int_0^L \sigma(\xi)\left[\frac{1}{\sqrt{\{(x-\xi)^2+R^2(x)\}}}-\frac{1}{\sqrt{\{(2h+x+\xi)^2+R^2(x)\}}}\right]\mathrm{d}\xi = V \quad (0<x<L). \quad (\mathrm{A}\,1)$$

The solutions for an isolated ellipsoid and for a one-parameter family of semi-infinite hyperboloids can be found by separation of variables. Otherwise, aside from inverse solutions, we must approximate on the basis that the needle is slender, using methods familiar from the aerodynamic theory of slender bodies.

We must first manipulate (A 1) to avoid divergent integrals. Adding and subtracting terms and integrating, following the procedure introduced into aerodynamics by Schultz-Piszachich (1951) and used also by Landau & Lifshitz (1960) for a similar electrostatic problem, gives

$$\sigma(x)\left[\sinh^{-1}\frac{x}{R}+\sinh^{-1}\frac{L-x}{R}+\sinh^{-1}\frac{2h+x}{R}-\sinh^{-1}\frac{2h+L+x}{R}\right]$$
$$-\int_0^L[\sigma(x)-\sigma(\xi)]\left[\frac{1}{\sqrt{\{(x-\xi)^2+R^2\}}}-\frac{1}{\sqrt{\{(2h+x+\xi)^2+R^2\}}}\right]\mathrm{d}\xi = V. \quad (\mathrm{A}\,2)$$

We can now approximate formally for small $R$ to obtain

$$\sigma(x)\ln\frac{4x(L-x)(2h+x)}{R^2(x)(2h+L+x)}-V=\int_0^L[\sigma(x)-\sigma(\xi)]\left[\frac{1}{|x-\xi|}-\frac{1}{2h+x+\xi}\right]\mathrm{d}\xi. \quad (\mathrm{A}\,3)$$

The neglected terms are formally of order $(a/L)^2$ or $(a/h)^2$, whichever is the greater, and for a smooth body this indicates the actual order of magnitude of the error. Near blunt ends the error is much greater over a short distance, but integrated effects are in error by only that order. (For example, (A 3) predicts constant charge

distribution along the entire length of an isolated ellipsoid, whereas it should actually extend only between the foci; but the capacity is affected only by a factor of order $(a/L)^2$.)

*Approximate charge distribution, capacity, and axial force*

To solve (A 3) for a general shape, we must accept a much greater error, of relative order $\{\ln(L/a)\}^{-2}$ or $\{\ln(h/a)\}^{-2}$. To that approximation the right-hand side of (3) is negligible, so that the charge distribution is

$$\sigma(x) = V \Big/ \ln \frac{4x(L-x)(2h+x)}{R^2(x)(2h+L+x)} \left[1 + O\left(\frac{1}{\ln^2(L/a)}, \frac{1}{\ln^2(L/h)}\right)\right]. \tag{A 4}$$

That the error is of the stated order can be verified, for example in the case of the isolated cylinder or isolated pointed parabolic-arc spindle, by recalculating the neglected terms.

The capacity $C$ of the needle is the total charge divided by its potential; in our approximation

$$C = \int_0^L \mathrm{d}x \Big/ \ln \frac{4x(L-x)(2h+x)}{R^2(x)(2h+L+x)}. \tag{A 5}$$

The attractive force between the needle and plane is most easily found from a virtual displacement at constant potential according to (Jeans 1925, p. 104).

$$F = \tfrac{1}{2} V^2 \partial C/\partial h. \tag{A 6}$$

This gives (with the sign reversed to make an attractive force positive)

$$F = V^2 \int_0^L \left(\frac{1}{2h+x} - \frac{1}{2h+L+x}\right) \mathrm{d}x \Big/ \left[\ln \frac{4x(L-x)(2h+x)}{R^2(x)(2h+L+x)}\right]^2. \tag{A 7}$$

(It is tempting to conjecture that for a needle with a long cylindrical midsection the two terms in (A 7) give the forces on the two ends.) These results remain valid, and simplify, in the limits $L \to \infty$ and $h \to \infty$, the force of course vanishing for an isolated needle.

*Semi-infinite paraboloid*

These equations reproduce known results for the isolated ellipsoid and semi-infinite hyperboloid. Another example for which all the integrations can be given

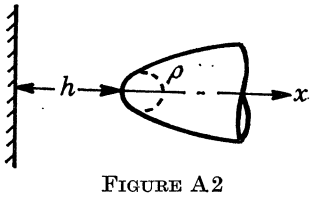


FIGURE A 2

explicitly is the semi-infinite paraboloidal needle (figure A 2). Putting $R(x) = \sqrt{(2\rho x)}$ where $\rho$ is the nose radius, gives the charge distribution

$$\sigma(x) = \frac{V}{\ln\{2(2h+x)/\rho\}}. \tag{A 8}$$

Near the vertex this agrees with the exact result for the hyperboloid of the same nose radius, except that the distribution should start at the focus rather than the vertex. The capacity is infinite, but the force is

$$F = \frac{V^2}{\ln(4h/\rho)}. \tag{A 9}$$

This vanishes as the wall recedes, in agreement with the exact solution for an isolated paraboloid.

*Ellipsoid*

For an ellipsoidal needle (figure A 3) with $R(x) = 2a\sqrt{\{x(L-x)/L\}}$, the charge distribution is

$$\sigma(x) = V \Big/ \ln \frac{L^2(2h+x)}{a^2(2h+L+x)}. \tag{A 10}$$

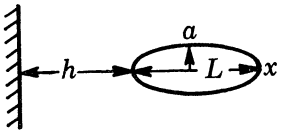


FIGURE A 3

Although the integral for the capacity has not been evaluated, that for the force gives

$$F = V^2 \left[ 1 \Big/ \ln \frac{2hL^2}{a^2(2h+L)} - 1 \Big/ \ln \frac{L^2(2h+L)}{a^2(2h+2L)} \right]. \tag{A 11}$$

As the length $L$ increases, the second term vanishes, and the first reproduces the result (A 9) for the semi-infinite paraboloid.

*Semi-infinite cylinder*

For other shapes, one must resort to numerical integration, or to further approximation. For $R = \text{const.} = a$ and $L = \infty$ (figure A 4) the charge distribution is

$$\sigma(x) = V \Big/ \ln \frac{4x(2h+x)}{a^2}. \tag{A 12}$$

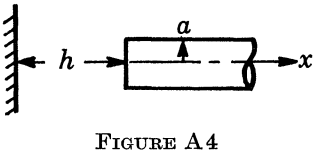


FIGURE A 4

This has violent fluctuations near the end, varying from zero at $x = 0$ to infinity at $x/a = a/8h$ and back to 1.4 V at twice that distance. However, all this detail is spurious, since the slender-body approximation breaks down where $x = O(a)$; and the fluctuations disappear if the end is rounded—for example, as a hemisphere. The capacity is again infinite; the force is given by

$$F = V^2 \int_0^\infty \mathrm{d}x \Big/ (2h+x) \left[ \ln \frac{4x(2h+x)}{a^2} \right]^2. \tag{A 13}$$

This has not been evaluated, but fairly close bounds are easily found. Except very near the end, the denominator is less than $(2h+x)\,[\ln 4(2h+x)^2/a^2]^2$ and greater than $(h+x)\,[\ln 4(h+x)^2/a^2]^2$, and this gives

$$\frac{V^2}{4\ln(4h/a)} < F < \frac{V^2}{4\ln(2h/a)}. \tag{A 14}$$

These are probably true bounds, because the gap between them is much greater than the error arising from our approximations. They are shown in figure 2, p. 455.

*Distant finite needle*

For any needle whose distance from the plane is not small compared with its length (including the isolated needle) (figure A 5), the integrals can be approximated

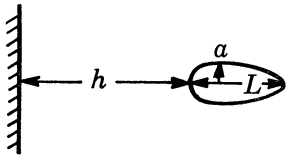


FIGURE A 5

in simple form, but with an increased error—of order $\{\ln(L/a)\}^{-1}$. The logarithm in (A 7) can be written as

$$\ln\frac{4x(L-x)\,(2h+x)}{R^2(x)\,(2h+L+x)} = 2\ln\frac{L}{a}\left[1+\frac{1}{2\ln(L/a)}\ln\frac{4x(L-x)\,(2h+x)\,a^2}{L^2(2h+L+x)\,R^2(x)}\right]. \tag{A 15}$$

The second term can be neglected with an error of relative order $(\ln L/a)^{-1}$ provided that $L/h$ is of order unity (i.e. not large). This gives

$$C = \frac{L}{2\ln(L/a)}\left[1+O\left(\frac{1}{\ln(L/a)}\right)\right], \tag{A 16$a$}$$

$$F = \frac{V^2}{\{2\ln(L/a)\}^2}\ln\frac{(2h+L)^2}{4h(h+L)}\left[1+O\left(\frac{1}{\ln(L/a)}\right)\right]. \tag{A 16$b$}$$

This force vanishes like $h^{-2}$ as the plane recedes, which is the correct behaviour, exemplified by a sphere (Jeans, p. 103). These approximations are easily seen to be true lower bounds for any shape no sharper than an ellipsoid—and hence, in particular, for a cylinder.

*Distant ellipsoid*

Higher approximations can be calculated for a distant needle of specified shape. Thus for the ellipsoid, using (A15) in (A5) gives

$$C = \frac{L}{2\ln(L/a)} + \frac{1}{\{2\ln(L/a)\}^2}[(2h+2L)\ln(2h+2L) + 2h\ln 2h - 2(2h+L)\ln(2h+L)] + \ldots. \tag{A 17}$$

Differentiating this gives only the previous first approximation (A16$b$) for the force.

Using (A 15) in (A 7) gives the second approximation

$$F = \frac{V^2}{\{2\ln(L/a)\}^2}\ln\frac{(2h+L)}{4h(h+L)}\left[1+\frac{1}{2\ln(L/a)}\ln\frac{h+L}{h}+\ldots\right]. \tag{A 18}$$

Expanding the full result (A 11) for large $h/L$ confirms this.

*Distant cylinder*

For a distant cylinder, the second approximation for the capacity is

$$C = \frac{L}{2\ln(L/a)}+\frac{1}{\{2\ln(L/a)\}^2}[2(1-\ln 2)L+2h\ln 2h + (2h+2L)\ln(2h+2L)-2(2h+L)\ln(2h+L)]. \tag{A 19}$$

In the limit $h/L\to\infty$ this reproduces the first two terms of the expansion for an isolated cylinder due to Hallén (1929),

$$\frac{C}{L} = \frac{1}{2\ln(L/a)}+\frac{2(1-\ln 2)}{\{2\ln(L/a)\}^2}+\frac{1.08676}{\{2\ln(L/a)\}^3}+\frac{5.5180}{\{2\ln(L/a)\}^4}+\ldots.$$

The second approximation for the force is

$$\frac{F}{V^2} = \frac{1}{\{2\ln(L/a)\}^2}\ln\frac{(2h+L)^2}{4h(h+L)}+\frac{1}{\{2\ln(L/a)\}^3}\left[\mathscr{L}_2\left(\frac{L}{2h+2L}\right)-\mathscr{L}_2\left(\frac{L}{2h+L}\right) - \ln 2\ln\frac{(2h+L)^2}{4h(h+L)}+\tfrac{1}{2}\ln^2\frac{2(h+L)}{L}-\ln^2\frac{2h+L}{L}+\tfrac{1}{2}\ln^2\frac{2h}{L}\right]+\ldots, \tag{A 20}$$

where $\mathscr{L}_2$ is the dilogarithm.

The curves shown in figure 2 were calculated from this approximation, but an attempt has been made to increase its accuracy by recasting the series according to

$$\frac{1}{\{2\ln(L/a)\}^2}A(h/L)+\frac{1}{\{2\ln(L/a)\}^3}B(h/L)\to\frac{A}{\{2\ln(L/a)-\frac{1}{2}(B/A)\}^2}. \tag{A 21}$$

This modification has been adopted because it is found to increase the accuracy of the two-term approximation in various special cases—such as the ellipsoid—where more accurate results are known for comparison. It was also used by Landau & Lifshitz (1960) in a similar problem. More generally, it seems to improve the second approximation in any perturbation problem where the solution proceeds in powers of $(\ln 1/\epsilon)^{-1}$; an example from viscous flow theory is a circular cylinder in a uniform stream at low Reynolds number, where Lamb's Oseen approximation for the drag—which implicitly involves the modification of (A 21)—is much more accurate than the straightforward two-term expansion of Proudman & Pearson (1957).

## References (Appendix)


Landau, L. D. & Lifshitz, E. M. 1960 *Electrodynamics of continuous media*, pp. 18–19. Oxford: Pergamon.

Proudman, I. & Pearson, J. R. A. 1957 *J. Fluid Mech.* **2**, 237.

Jeans, J. H. 1925 *The mathematical theory of electricity and magnetism* (5th ed.). Cambridge University Press.

Hallén, E. 1929 *Ark. Astr. Fys.* **21** A no. 22.

Schultz-Piszachich, W. 1951 *Österr. Ing. Arch.* **4**, 289.